Batch fabricated scanning near field optical microscope/atomic force microscopy microprobe integrated with piezoresistive cantilever beam with highly reproducible focused ion beam micromachined aperture

P. Grabiec[a)]
Institute of Electron Technology, Warszawa, Poland

J. Radojewski
Wroclaw University of Technology, Wroclaw, Poland

M. Zaborowski and K. Domanski
Institute of Electron Technology, Warszawa, Poland

T. Schenkel
E.O. Lawrence Berkeley National Laboratory, Berkeley, California

I. W. Rangelow
University of Kassel, Kassel, Germany

(Received 30 June 2003; accepted 20 October 2003; published 24 December 2003)

In scanning near field optical microscope (SNOM), an optical probe with aperture diameter well below the optical wavelength is moved over the sample. The sample-probe distance control is one of the key problems in SNOM. Our earlier approach allowed for fabrication of the piezo-SNOM/atomic force microscopy (AFM) probe, however, reproductivity of the process and optical quality of the device were not satisfactory. Now we report an innovative processing sequence, which offers highly reproductive batch processing, typical for semiconductor technology and renders it possible to produce cantilevers playing role of an AFM detector as well as a nanoaperture detector. Moreover, illumination of the aperture is easier because of a wide input opening and its big cone angle. The throughput is in the range of 10^{-5} and higher. Apertures in hollow pyramids have been formed by direct ion beam drilling with a focused beam of 30 keV Ga^+ ions. Direct focused ion beam (FIB) drilling is a reproducible process for hole formation at the 30–100 nm diameter range. Formation of smaller apertures is possible if a special FIB drilling/deposition procedure is applied.
© *2004 American Vacuum Society.* [DOI: 10.1116/1.1633280]

I. INTRODUCTION

In scanning near field optical microscope (SNOM), an optical probe with aperture diameter (Φ) well below the optical wavelength is moved just over the sample (typical aperture diameter is approximately 50 nm). The probe forms a local subwavelength light source, a detector, or a scattering center. So small (nanometric) a light source illuminates a sample surface, which gives optical information on the surface with a nanometric resolution. The sample-probe distance control is one of the key problems in SNOM. For this purpose a strong distance-dependent signal should be applied in closed loop feedback. In early SNOM installations the scanning tunneling microscope mechanism was used. In that solution the sample should be specially prepared to conduct an electrical tunnel current.[1] Nowadays a shear-force feedback mechanism[2] is dominant. This technique uses an optical fiber probe, which vibrates parallel to the surface under test in its dominant mechanical resonance. The vibration amplitude is a few nanometers. The amplitude and phase change due to tip-surface distance variation is used for distance regulation. The tips usually used in this method are tapered optical fibers coated with metal film in such a way that the very end of the tip is free from the metal layer. Unfortunately, the fabrication process renders very small angles of the apex. It results in significant squeezing of the light passing through the tapered region and the aperture itself. In Fig. 1 we show the throughput of the aperture size 10, 20, and 100 nm versus the apex angle. Values used to plot curves for

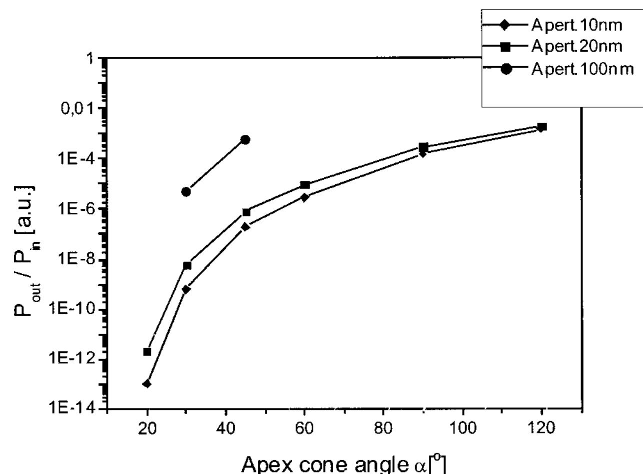

FIG. 1. Transmission coefficient of an aperture probe as a function of the full taper cone angle α (after Ref. 3).

a)Electronic mail: grabiec@ite.waw.pl

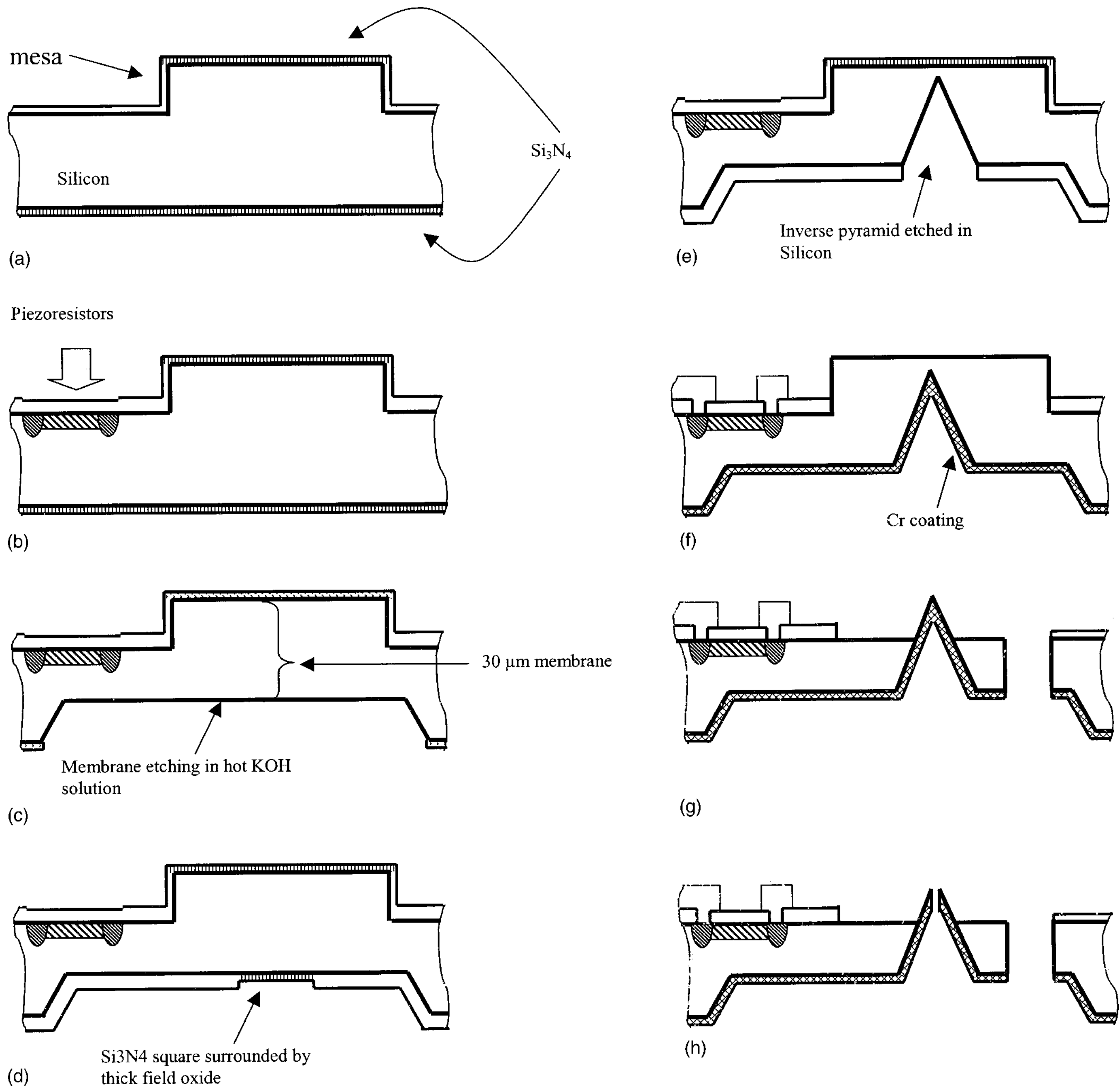

FIG. 2. Scheme of the process sequence of the microprobe fabrication.

a 10 and 20 nm aperture were calculated using the multiple multipole method to solve Maxwell's equations. Transmission coefficient for a 100 nm aperture diameter was approximated by scaling the numerical data according to the Bethe/Bouwkamp model.[3] One can easily find the rapid increase of P_{in}/P_{out} ratio by the factor of 10^7 when the apex angle changes from 20° to 60°, practically independent from the aperture size. The second problem of shear-force distance regulation microscopic systems is limited resolution due to lateral vibration of the tip. It has to be noted, however, that in the case of SNOM the resolution is limited by aperture diameter itself rather than by shear-force mechanism.

We developed a combined piezoresistive SNOM/atomic force microscopy (AFM) probe, which enables precise detection of force interactions acting on the microtip. Moreover, the angle of the apex cone is close to 50°, which renders it possible to obtain a high aperture transmission coefficient. The results on the probe construction, manufacturing, and its basic optical parameters are described later. Results of piezoresistor bridge measurements were published elsewhere.[4–6]

II. FABRICATION

Our earlier approach[2] allowed for fabrication of the piezo-SNOM/AFM probe, however, reproductivity of the process

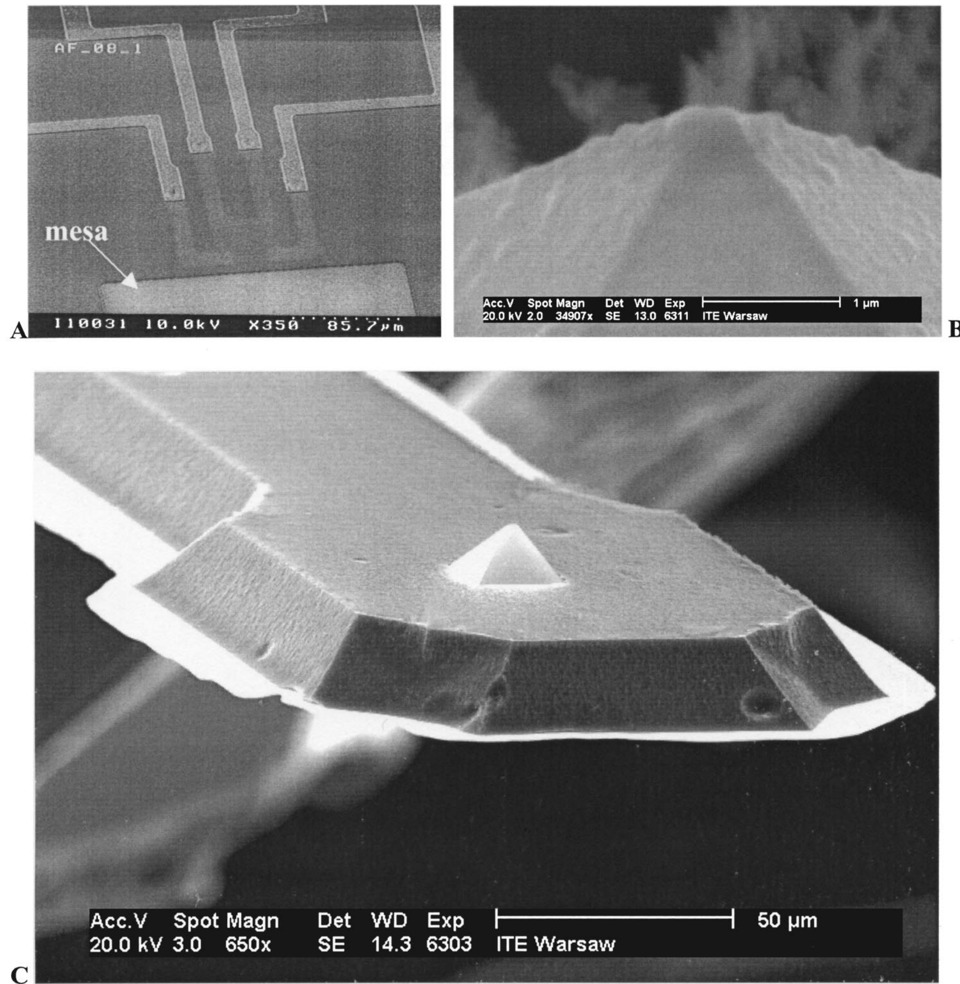

FIG. 3. SEM images of the piezoresistor set (a), the pyramid tip (b), and the beam end with pyramid (c).

and optical quality of the device were not satisfactory. Therefore, basing on our experiences and considering reported examples[7–10] we have developed an innovative processing sequence, which offers highly reproductive batch processing, typical for semiconductor technology and silicon micromechanics and renders it possible to produce cantilevers playing role of an AFM detector as well as an optical photodetector or nanoaperture detector.

A number of functional components were integrated in one silicon chip to form the microprobe. The microprobe forms a cantilever beam with a hollow pyramid at the end. A set of force sensitive piezoresistors, placed in the base of the beam, allows for detection of small deflections of the beam. A tip-shape platform acts as an atomic force-sensitive unit and a nanohole in the platform serves for the near field optical measurements.

The fabrication process starts from pad oxide formation followed by low-pressure chemical vapor deposition (LPCVD) nitride deposition. Then a rectangular mesa in a future beam area is defined and etched—Fig. 2(a). The mesa level remains several micrometers elevated over the whole surface. Next, a sequence of oxidation, photolithography, and implantation is used to form a set of piezoresistors in the base of the beam area—Fig. 2(b). Postimplantation oxidation is optimized to effectively protect the probe surface against later etching processes.

In the next step, membrane areas are defined in the nitride film at the backside of the wafer, and subsequently etched in a hot KOH solution while the front side of the wafer is protected by a special chuck. The membrane thickness of 30 μm (as measured in the thickest, i.e., mesa area) is achieved by the etching—Fig. 2(c).

In the following sequence an inverse pyramid hollow is created. First, a thin nitride layer is LPCVD deposited. A square shape is photolithographically defined at the backside of the membrane, in the future tip location, using the SU-8 process, followed by thick oxidation, resulting in the LOCOS-like shape—Fig. 2(d). SU-8 is a commercially available very thick negative photoresist (up to 1 mm) allowing for fabrication of vertical edges of the pattern.[11] Next, both the nitride and oxide layers are dry-etched away from the square area at the backside of the membrane. Finally, an inverse pyramid hollow is etched in this place where bare silicon was previously exposed—Fig. 2(e).

The photolithographic opening of contacts to piezoresistors followed by creation metal connections in standard complementary metal–oxide–semiconductor integrated cir-

FIG. 4. SEM image of tip shape and aperture obtained by the FIB method.

cuits processing sequence completes of formation of piezoresistor set. Then, the backside of the membrane, including pyramid walls, is covered with a chromium layer in a magnetron sputtering process—Fig. 2(f). In the next step, a probe shape is photolithographically defined at the front side of the wafer, followed by silicon plasma etching and chromium etching. Finally, a mask-less plasma etching of the nitride/pad oxide sandwich from the top of the mesa structure is performed, followed by a deep plasma silicon etching, resulting in exposition of the metal pyramid in the former mesa area—Fig. 2(g). Scanning electron microscopy (SEM) images of the main microprobe regions are shown in Fig. 3.

The creation of a small aperture of several tens of nanometers is the last step of the SNOM/AFM microprobe fabrication. A focused ion beam (FIB) direct ion beam drilling with a focused beam of 30 keV galium ions is applied to produce a hole in the hollow chromium pyramid tip—Fig. 2(h). Direct FIB drilling is a reproducible process for formation of the hole at the 30–100 nm diameter range—Fig. 4. The ion dose for sputtering of the hole is about 2×10^9 ions. Positions of specimens in regular arrays can be dialed in automatically, enabling rapid processing of the samples. FIB drilling experiments indicate an aspect ratio limit of about 5:1, but the hole size is not dependent of the aspect ratio for

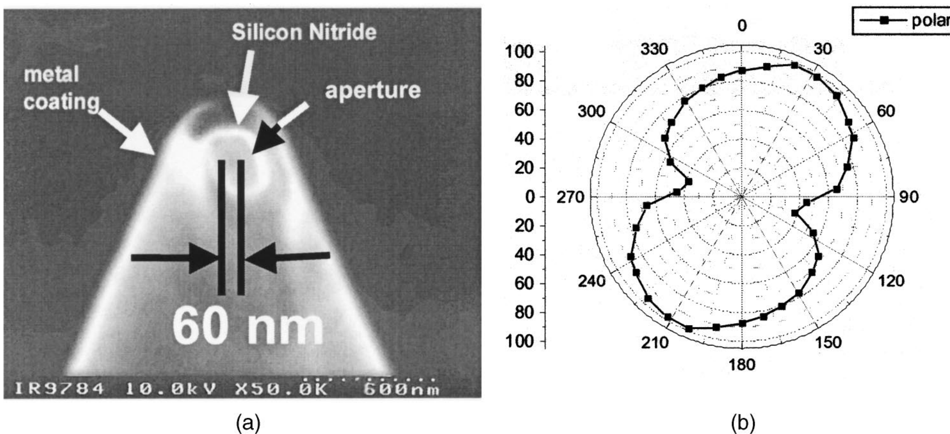

FIG. 5. SNOM nanoaperture probe (see Ref. 14) from authors laboratory (2001)—(a) and a polarization ratio of 60/80 nm aperture with elliptical shape—(b).

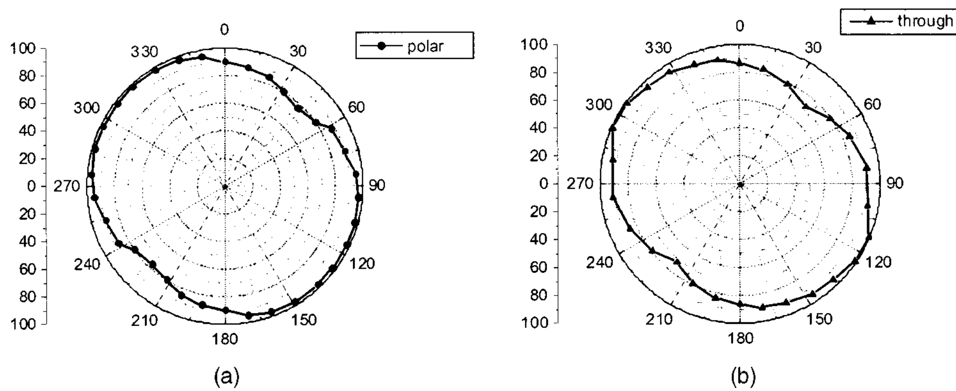

FIG. 6. Polarization ratio of 50 nm aperture fabricated with improved (present) technology—(a) and relative throughput of 50 nm aperture—(b).

hole below a diameter of 100 nm. The available FIB systems equipped with an *xy* stage and image recognition allow drilling 360 sensor Cr pyramids on the wafer for a reasonably short time with excellent reproducibility (size deviation and circularity).

III. MEASUREMENTS

Looking at the SEM images of two tips etched by the described FIB method [Figs. 4(a) and 4(b)], one can observe a well defined aperture on the end face of the pyramidal shaped tip placed on the end of the piezoelectric cantilever. For final verification of our tips we performed polarization measurements in the far field. For this purpose we used a helium–neon laser light with a beam power of $P=5$ mW and wavelength of $\lambda=0.6328$ μm. The light beam was coupled to the aperture via microscopic objective of numerical aperture (NA)=0.5. We used a $\lambda/4$ plate to change linear polarization coming from our laser to a circular one to have a possibility to control the input light polarization via a rotating polarizer. The degree of polarization of the light, which passed the nanoaperture, was controlled by an analyzer placed between the aperture and the photomultiplier.

From a theoretical point of view[12] an ideally symmetrical aperture possesses two peaks of intensity associated with depolarization fields. They are generated in the regions where an incident field is normal to the core/coating interface. Depolarization fields rotate following the orientation of the incident light polarity. As a result, symmetrical behavior should be observed in far field for symmetrical apertures. An elliptical or rough rim of the aperture coming from metal grains strongly changes the field distribution resulting in asymmetry in far field.[13]

In the beginning of our measurements we tested cantilevers elaborated in our laboratory in 2001, described in Ref. 14. After precise measurements of the aperture we discovered its elliptical shape. In Fig. 5(a) a SEM image of the 60/80 nm tip aperture was shown and in Fig. 5(b)—corresponding polarization ratio graph. We found out that the minimum polarization ratio was about 1:38 and the maximum above 1:98. In these structures the light was transmitted through a channel fabricated by etching inside a steep SNOM pyramid formed by ⟨338⟩ crystal planes with an aperture created by FIB slicing. This technique did not allow for good control of circularity of the aperture. After improving our technology we expected to obtain better results (minimum-maximum polarization ratio difference factor less than 2) involved by better circularity of the aperture opening formed by FIB drilling. Figure 6(a) presents a relative polarization ratio for aperture fabricated using our batch technology. In this case we found polarization ratio values lying between 1:77 and 1:98. Thus, a significant improvement of the optical properties of our SNOM cantilevers was confirmed. The improvement of both—changing of pyramid fabrication.

As we mentioned in Sec. I, the transmission coefficient of the apertures shows strong reliance on its diameter. For example, for a cone angle 50° starting from a factor of 10^{-3} for the aperture diameter of 100 nm down to a factor 5×10^{-7} for an aperture diameter of 10 nm. In our case we obtained a 50 nm aperture throughput ratio of 5×10^{-5} with values lying within 30% in respect to the polarization direction [Fig. 6(b)].

IV. SUMMARY

We elaborated cantilever technology, which combines a conventional AFM piezoresistive cantilever with a nanoaperture on the very apex of a hollow metal pyramid located on its end. It leads to better sample-tip distance control than that obtained by the conventional shear-force technique. Moreover, illumination of the aperture is easier because of a wide input opening and its big cone angle. It makes it possible to use a conventional microscopic objective with a high NA and low internal stresses for coupling the light and for use in polarization dependent experiments. The throughput is in the range of 10^{-5} and higher. We can use a lower illumination beam energy in that case to avoid heating of the nanoaperture by light beam energy. A high aperture transmission ratio simplifies the detection of the optical signal after interaction with the sample by a rising signal-to-noise ratio.

Presented at the 47th International Conference on Electron, Ion, and Photon Beam Technology and Nanofabrication, Tampa, FL, 27–30 May 2003.

[1]D. Pohl, W. Denk, and M. Lanz, Appl. Phys. Lett. **44**, 651 (1984).
[2]E. Betzig, P. Finn, and S. Weiner, Appl. Phys. Lett. **60**, 2484 (1992).
[3]B. Hecht, B. Sick, and U. P. Wild, J. Chem. Phys. **112**, 7761 (2000).

[4]T. Gotszalk, R. Linemann, I. W. Rangelow, P. Grabiec, and P. Dumania, Int. J. Electron. **34**, 34 (1996).
[5]T. Gotszalk, P. Grabiec, and I. Rangelow, Ultramicroscopy **82**, 39 (2000).
[6]P. Grabiec, T. Gotszalk, and I. W. Rangelow, Microelectron. Eng. **46**, 405 (1998).
[7]H. Zhou, A. Midha, L. Bruchhaus, G. Mills, L. Donaldson, and J. M. R. Weaver, J. Vac. Sci. Technol. B **17**, 1954 (1999).
[8]T. Gotszalk, P. Grabiec, and I. W. Rangelow, Ultramicroscopy **82**, 39 (2000).
[9]S. A. C. Gould *et al.*, Ultramicroscopy **33**, 93 (1990).
[10]D. A. Walters, J. P. Cleveland, N. H. Thomson, P. K. Hansma, M. A. Wendman, G. Gurley, and V. Elings, Rev. Sci. Instrum. **67**, 3583 (1996).
[11]http://www.microchem.com/products/su_eight.htm.
[12]O. J. F. Martin and M. Paulus, J. Microsc. **205**, 147 (2002).
[13]T. Lacoste, T. Huser, R. Prioll, and H. Heinzelman, Ultramicroscopy **71**, 333 (1998).
[14]P. Grabiec, T. Gotszalk, J. Radojewski, K. Edinger, N. Abedinov, and I. W. Rangelow, Microelectron. Eng. **61–62**, 981 (2002).